Growth Kinetics of Nanocrystalline ZnO Particles from Colloidal Suspensions

Eva M. Wong,[†] John E. Bonevich,[‡] and Peter C. Searson*[,†]

Department of Materials Science and Engineering, The Johns Hopkins University, Baltimore, Maryland 21218, and Metallurgy Division, National Institute of Standards and Technology, Gaithersburg, Maryland 20899

Received: May 28, 1998

Colloidal chemistry techniques were used to synthesize ZnO particles in the nanometer size regime. The particle aging kinetics were determined by monitoring the optical band edge absorption and using the effective mass model to approximate the particle size as a function of time. We show that the growth kinetics of the ZnO particles follow the Lifshitz−Slyozov−Wagner theory for Ostwald ripening. In this model, the higher curvature and hence chemical potential of smaller particles provides a driving force for dissolution. The larger particles continue to grow by diffusion-limited transport of species dissolved in solution.

Introduction

Many examples of quantum state semiconductor systems, including ZnO, CdS, ZnS, PbS, CdSe, and TiO_2, can be found in the literature.[1−11] The optical properties of these materials have been of particular interest since confinement of charge carriers in the restricted volume of small particles can lead to effects such as enlargement of the band gap.[12−20] Several excellent reviews of the optical properties of nanoparticles can be found in the literature.[21−23]

Colloidal chemistry techniques have been used to prepare a wide variety of particles in the nanoscale regime, and various surface stabilization schemes have been adopted to produce well-dispersed solutions.[1,2,11,24] However, despite the large number of reports in the literature on the synthesis and photochemical properties of nanoparticles, surprisingly little is known about the growth kinetics of these systems. A detailed understanding of the growth behavior of these systems is essential for control of particle sizes and hence optical properties.

Zinc oxide is of interest for use as a phosphor material in display applications. Although many excellent cathode ray phosphors exist presently, the increasing demand for portable display devices has generated interest in materials that can operate efficiently at low voltages. Cathode ray devices operate at greater than 10 keV, whereas field emitter displays are required to operate in the range 10−1500 eV.[25] Phosphors such as zinc-doped zinc oxide (ZnO:Zn) can be excited at relatively low voltages, and while efficiencies of 15−20% can be obtained above 10 keV for many cathode ray phosphors, only the ZnO:Zn system has demonstrated reasonable (1−5%) efficiencies at low voltages (10−50 eV).[25] Furthermore, in contrast to the case of high-voltage phosphors where larger particle size is needed for higher efficiency, it has been suggested recently that the cathodoluminescence of small-sized phosphors is superior to large-sized phosphors under low-voltage excitation.[26]

Zinc oxide colloids have been prepared using many techniques: controlled double-jet precipitation,[27] sol−gel synthesis,[28] chemical precipitation,[29] and colloidal synthesis.[30] While many reports have focused on the synthesis and characterization of quantum size particles, there have not been any detailed studies of the growth process. In this paper we show that the growth of the ZnO particles in this system is diffusion-dependent and follows Ostwald ripening kinetics according to Lifshitz−Slyozov−Wagner (LSW) theory.

Experimental Procedure

Preparation of the ZnO colloidal suspensions followed the method of Bahnemann and Hoffmann.[30] For a typical preparation, 1 mmol of zinc acetate dihydrate ($Zn(CH_3CO_2)_2 \cdot 2H_2O$; Aldrich,[31] reagent grade) was dissolved in 80 mL of 2-propanol (Aldrich, spectrophotometric grade) under vigorous stirring at 50 °C and subsequently diluted to a total volume of 920 mL followed by chilling to 0 °C. An 80 mL aliquot of a 2×10^{-2} M NaOH (Aldrich, reagent grade) solution in 2-propanol was then added to the $Zn(OAc)_2$ solution at 0 °C within 1 min under constant stirring. Water was distilled and purified (Millipore Milli-Q System) to a resistivity of 18 MΩ cm. The suspension was then immersed in a preheated water bath for up to 2 h. Upon removal from the water bath, the suspension was covered and stored at room temperature. These dispersions remained transparent and stable for periods of up to a few months at which time they became translucent followed by the appearance of a fine white precipitate which ultimately settled to the bottom of the container.

Particle sizes were determined using a JEOL3010 HRTEM (high-resolution transmission electron microscope). The microscope, operated at 300 keV, has a spatial point-to-point resolution of 0.17 nm. Samples were prepared by placing a drop of the colloidal suspension on a holey carbon-coated 2.3 mm copper grid for 30 s. The excess liquid was then removed, and the specimens were allowed to dry by evaporation in air.

Crystal structure identification was made by X-ray diffraction using a Phillips model APD1700 diffractometer with Cu Kα radiation. Powder diffraction samples were prepared by rotary evaporation of the suspension to a fine powder. The ZnO powder was collected and then dried in an oven heated to 200 °C for 2 h under a constant flow of oxygen. Subsequently, the powder was pressed into a zero background quartz sample holder (The Gem Dugout Co., State College, PA) without addition of a binding agent. Extended time scans were performed in a limited 2θ region to determine the crystallite size using the Scherrer peak broadening method.[32]

[†] The Johns Hopkins University.
[‡] National Institute of Standards and Technology.

S1089-5647(98)02397-9 CCC: $15.00
Published on Web 09/11/1998

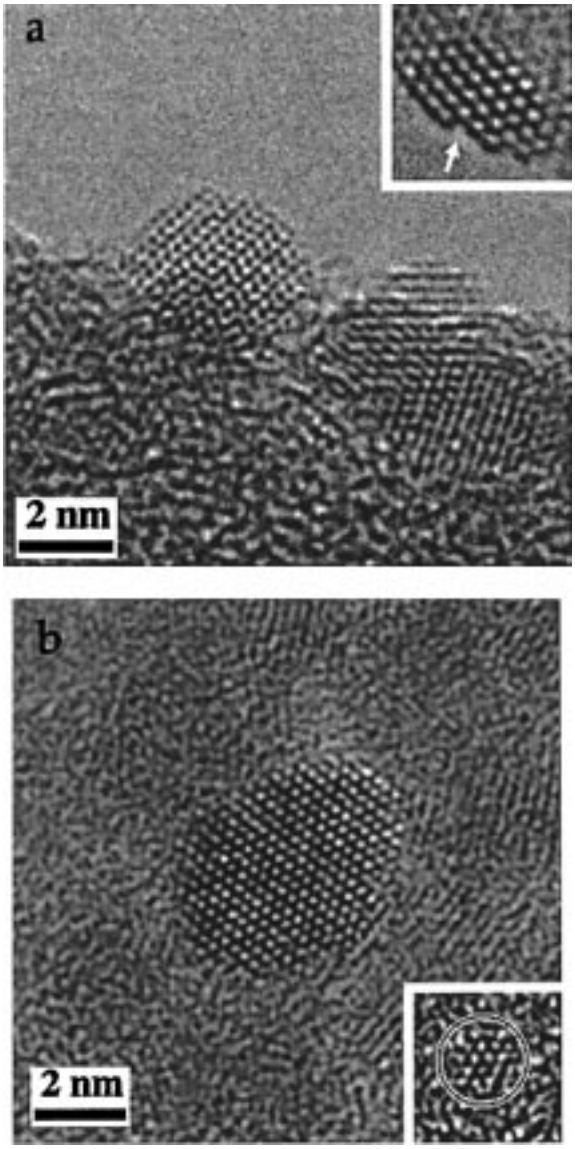

Figure 1. High-resolution transmission electron micrographs of ZnO particles aged at 35 °C for 2 h. (a) shows three particles about 3.7 nm in diameter and approximately spherical in shape. The particle shown in the inset demonstrates strong facetting with a surface step consisting of a single atomic layer (arrowed). (b) shows a single-crystal ZnO particle that exhibits evidence of facetting, and the inset shows a ZnO particle approximately 1.5 nm in diameter. Particles smaller than 1.5 nm could not be resolved due to insufficient contrast with the carbon film.

Absorption spectra were recorded using a Shimadzu UV-2101PC scanning spectrophotometer. Samples were withdrawn during aging in the water bath at predetermined time intervals by removal of 20 mL aliquots of the suspension. A blank solution of 2-propanol was used as the reference.

The concentration of Zn^{2+} in the colloidal suspensions was determined by atomic absorption spectroscopy of solution isolated from the ZnO particles by dialysis. Dialysis was performed by placing 125 mL of the colloidal solution in a Spectra/Por dialysis membrane encapsulated by means of a dialysis closure at either end. The dialysis bag containing the colloidal suspension was then placed into a 500 mL volume of the solvent (2-propanol) and rotated using a magnetic stirrer. The suspension was allowed to equilibrate with the dialysis fluid over a period of 3 days. The dialysis fluid was then extracted and analyzed using atomic absorption spectroscopy (Perkin-Elmer AS 4000).

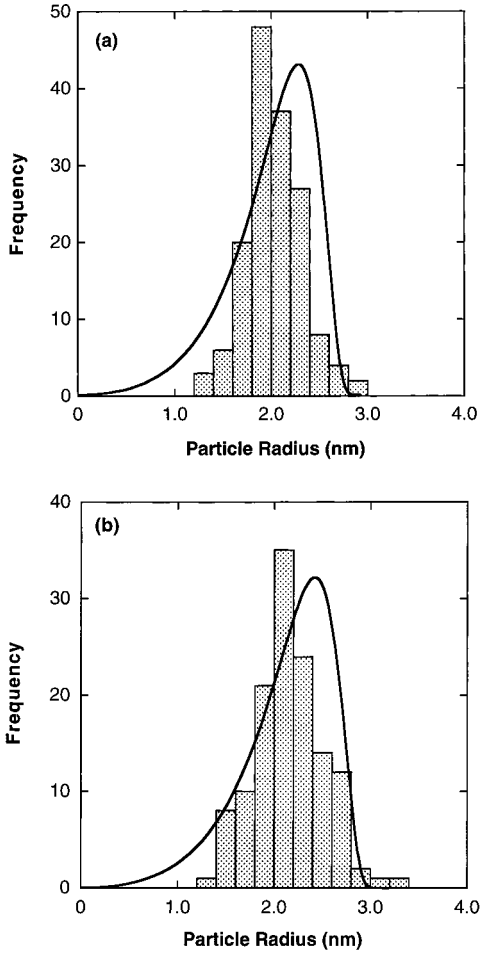

Figure 2. Histograms of the particle size distributions obtained from HRTEM images for ZnO colloids aged at (a) 35 and (b) 65 °C for 2 h. Overlayed is the theoretical distribution calculated from LSW theory.

Results and Discussion

Particle Size Determination and Distribution. *Transmission Electron Microscopy.* High-resolution transmission electron microscopy provides the most direct measurement of particle size for these colloids. Colloids aged at 35 °C for 2 h and 65 °C for 2 h were selected for particle size determination by HRTEM. Typical HRTEM images of particles obtained from a colloid aged at 35 °C are shown in Figure 1. While the particles are predominantly spherical in shape, many also exhibit surface facetting, as shown in the inset of Figure 1a where a step of one atomic layer can be seen. We note that particle sizes of less than about 1.5 nm could not be obtained since the contrast between the particle and the carbon support was not well defined in this size range (see Figure 1b inset).

Parts a and b of Figure 2 show the particle size distributions after aging at 35 and 65 °C for 2 h, respectively, obtained from analysis of more than 125 particles per sample. The number-weighted average particle diameter obtained from a colloid aged at 35 °C was determined to be 3.8 ± 0.2 nm whereas that obtained from a colloid aged at 65 °C was determined to be 4.2 ± 0.2 nm.

X-ray Diffraction. Figure 3 shows an X-ray powder diffraction pattern of a colloid aged at 65 °C for 2 h. The diffraction pattern exhibits the main peaks for the zincite form of ZnO as well as several other peaks, probably due to residual salts from the solution.

From the ZnO diffraction peak at $2\theta = 62.86°$ (see Figure 3), the volume-weighted average particle diameter obtained from

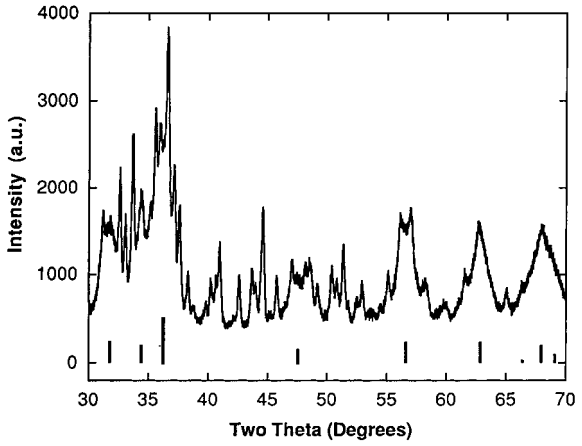

Figure 3. Powder X-ray diffraction pattern for ZnO particles aged at 65 °C for 2 h. The reference peaks for the zincite structure are also indicated.

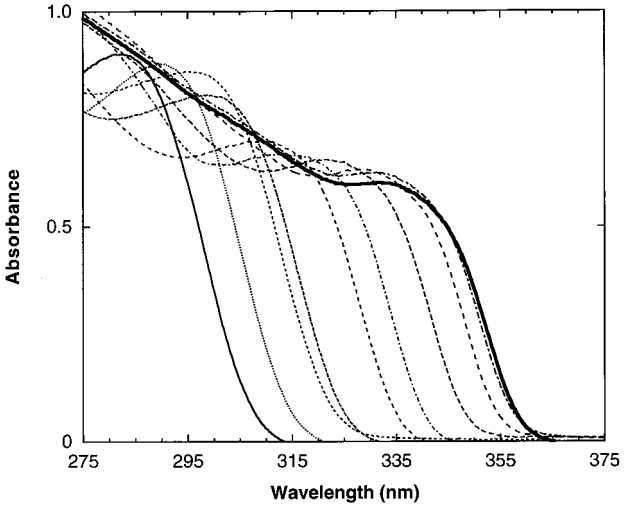

Figure 4. Absorption spectra for a colloid aged at 65 °C. The spectra were recorded at 0, 1, 3, 5, 10, 15, 30, 60, 90, and 120 min after immersion in the aging bath.

X-ray line broadening measurements was determined to be 6.02 nm. This value corresponds to the tail of the particle size distribution determined from HRTEM micrographs (Figure 2b) and is close to the value of 6.2 nm obtained from the absorption data (see next section). Detailed analysis of the line broadening for all aging temperatures and times was not performed due to the difficulty in obtaining sufficiently high-quality diffraction patterns.

Absorption Spectra. An example of the absorption spectra recorded during aging of a stable transparent colloidal suspension at 65 °C is shown in Figure 4. During aging for 2 h at a given aging temperature, the absorption edge progressively red-shifts toward 365 nm, corresponding to the bulk band gap for ZnO of 3.4 eV. It can be clearly seen that the growth of the particles is dependent on temperature and time. In addition, it can be seen that the spectral shift is retarded toward the end of the aging process and that the extent of this shift declines with decreasing aging temperature. These factors suggest that the aging conditions strongly affect the particle size and hence the optical properties.

To study the kinetics of the growth process, it is necessary to determine the particle size as a function of time for different aging temperatures. For convenience, we use the particle size inferred from the absorption edge. Although this approach has certain limitations, the particle size obtained from the absorption

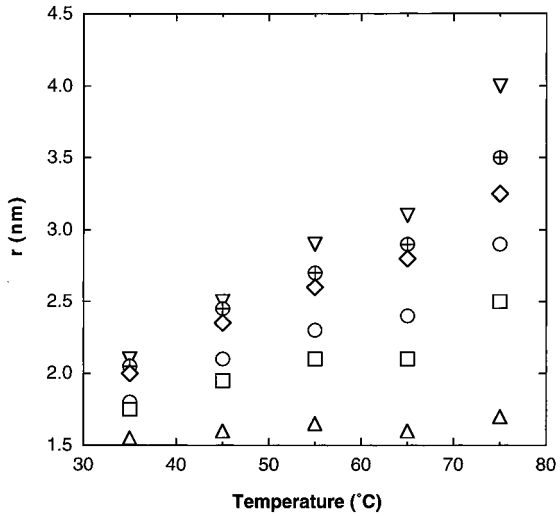

Figure 5. Particle radius calculated from absorption measurements versus temperature after aging for (△) 1, (□) 15, (○) 30, (◇) 60, (⊕) 90, and (▽) 120 min.

edge was slightly larger than the most probable value obtained from analysis of the HRTEM images and hence represents a reasonable approximation for kinetic analysis.

The average particle size as a function of time was determined from the absorption spectra using the effective mass model derived by Brus.[33−38] In the strong-confinement regime, the confinement energy of the first excited electronic state can be approximated by

$$E^* \cong E_g^{\text{bulk}} + \frac{\hbar^2\pi^2}{2r^2}\left(\frac{1}{m_e^* m_0} + \frac{1}{m_h^* m_0}\right) - \frac{1.8e^2}{4\pi\epsilon\epsilon_0 r} - \frac{0.124e^4}{\hbar^2(4\pi\epsilon\epsilon_0)^2}\left(\frac{1}{m_e^* m_0} + \frac{1}{m_h^* m_0}\right)^{-1} \quad (1)$$

where E_g^{bulk} is the bulk band gap, $\hbar$ is Planck's constant, r is the particle radius, m_e^* is the effective mass of electrons, m_h^* is the effective mass of holes, m_0 is the free electron mass, e is the charge on an electron, ϵ_0 is the permittivity of free space, and ϵ is the relative permittivity. The particle size was obtained from the band gap inferred from the optical absorption spectra taking $E_g^{\text{bulk}} = 3.4$ eV, $m_e^* = 0.24$, $m_h^* = 0.45$, and $\epsilon = 3.7$.[35]

Figure 5 shows a plot of the calculated particle size as a function of the aging temperature taken at increasing time intervals for the five aging temperatures studied. As described above, the particle size obtained by this method was slightly larger than the most probable particle size obtained from HRTEM images. For example, from Figure 5 it can be seen that the particle radius for a colloid aged at 65 °C for 2 h is 3.1 nm. This can be compared to the most probable value of 2.1 nm from the particle size distributions shown in Figure 2. The slightly larger particle sizes obtained from the absorption edge may be due to the assumptions used in the effective mass model or the values used for the constants[35] in eq 1. We note that other groups have reported that the effective mass model gives particle sizes somewhat larger than those obtained by direct measurement, such as HRTEM or X-ray line broadening,[7,41] and in some cases, the tight binding model has been shown to give closer agreement with experimental data.[13,42,43] In addition, we note that the absorbance may be related to the size distribution of the particles rather than the selection rule for absorption, in which case the particle size obtained by this method would be expected to be slightly larger than the average

particle size. In any case, as long as the particle size obtained from the absorption edge corresponds to the same point in the size distribution, this should be a reasonable value to use for analysis of the growth kinetics.

Particle Growth Kinetics. Coarsening effects due to capillary forces at phase boundaries are generally termed Ostwald ripening.[44−46] Lifshitz and Slyozov[45] and Wagner[46] developed a rigorous mathematical approach to Ostwald ripening, referred to as the LSW theory, in which either mass transport or reaction at the interface is the rate-limiting step.

For a species present at a solid/liquid interface, the local equilibrium concentration of the species in the liquid phase is dependent on the local curvature of the solid phase. Differences in the local equilibrium concentrations, due to variations in curvature, set up concentration gradients that lead to transport of species from the regions of high concentration (high curvature) to regions of low concentration (low curvature). These capillary forces provide the driving force for the growth of larger particles at the expense of smaller particles.

The concentration of a species in a liquid phase in equilibrium with a spherical solid particle is given by the Gibbs−Thomson equation:

$$C_r = C_\infty \exp\left(\frac{2\gamma V_m}{RT}\frac{1}{r}\right) \quad (2)$$

where C_r is the equilibrium concentration for a particle of radius r, C_∞ is the equilibrium concentration at a flat surface, γ is the interfacial energy, V_m is the molar volume of the solid phase, R is the gas constant, and T is the temperature. Considering only first-order terms (i.e., small deviations from the bulk concentration), we can write

$$C_r = C_\infty + \left(\frac{2\gamma V_m C_\infty}{RT}\frac{1}{r}\right) \quad (3)$$

For diffusion-controlled growth, the flux of a species to a growing particle can be obtained by considering Fick's first law in spherical geometry. For the case where the diffusion length is much greater than the particle radius

$$J = -D(4\pi r^2)\left(\frac{C_b - C_r}{r}\right) = -D4\pi r\left(C_b - C_\infty - \frac{2\gamma V_m C_\infty}{RT}\frac{1}{r}\right) \quad (4)$$

where D is the diffusion coefficient and C_b is the bulk concentration at sufficiently large distances from the particle.

The flux of species to a growing particle must obey the conservation of mass such that

$$J = \frac{1}{V_m}\frac{dV}{dt} = \frac{4\pi r^2}{V_m}\frac{dr}{dt} \quad (5)$$

The growth law can be obtained by combining eqs 4 and 5 and integrating over the appropriate boundary conditions. For a system of highly dispersed particles where the growth is controlled by diffusion, the rate law is given by

$$\bar{r}^3 - \bar{r}_0^{\,3} = Kt \quad (6)$$

where $\bar{r}$ is the mean particle radius and $\bar{r}_0$ is the initial particle radius. The constant K is given by

$$K = \frac{8\gamma D V_m^{\,2} C_\infty}{9RT} \quad (7)$$

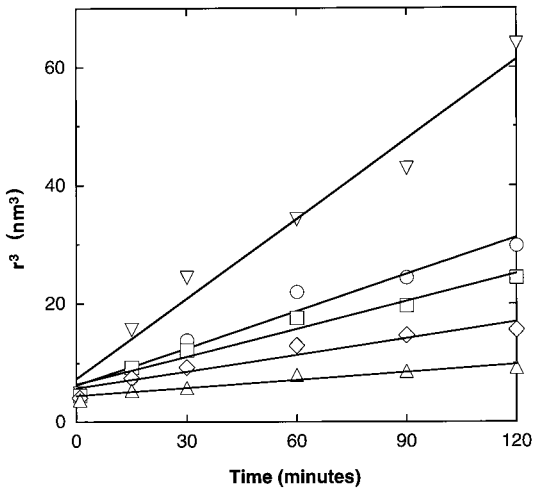

Figure 6. Cube of the particle radius versus aging time for (△) 35, (◇) 45, (□) 55, (○) 65, and (▽) 75 °C.

Figure 6 shows the cube of the particle radius plotted versus aging time for the different aging temperatures. From this figure it can be seen that the particle growth follows the Ostwald ripening growth law.

Further confirmation of the Ostwald ripening model can be obtained by consideration of the constant K. Since γ and V_m can be taken from the literature and C_∞ can be determined experimentally, values for the diffusion coefficient, D, can be obtained from the slopes in Figure 6 and compared to the Stokes−Einstein model. A value for the interfacial energy of 0.24 mJ/m^2 was assumed.[47] The concentration of Zn^{2+} in solution, C_r, for a colloids aged at 65 °C for 2 h was found to be 1.63×10^{-7} mol/L from atomic absorption spectroscopy of the dialysed solution. Since the concentration difference is relatively small ($2\gamma V_m/RTr \ll 1$), we make the approximation that $C_\infty \approx C_r$. Figure 7 shows the diffusion coefficient obtained from eqs 6 and 7 versus reciprocal temperature. From this figure it is seen that the diffusion coefficient obtained from the value of K is on the order of 10^{-5} cm^2/s, consistent with typical values for ions in solution at room temperature.[48,49]

The diffusion coefficient for Zn^{2+} obtained from the Ostwald ripening model can be compared to the Stokes−Einstein model for ionic diffusion:

$$D = \frac{kT}{6\pi\eta a} \quad (8)$$

where η is the viscosity of the solvent, a is the hydrodynamic radius of the solute, and kT has the usual meaning. The viscosity for 2-propanol as a function of temperature is known,[48] and the hydrodynamic radius for Zn^{2+} in methanol is 0.51 nm.[50] The temperature dependence of the diffusion coefficient obtained from eq 8 is shown in Figure 7. Comparison of the diffusion coefficients obtained from the experimental data using the LSW model and the Stokes−Einstein equation shows good agreement, providing further confirmation of the Ostwald ripening model for the growth kinetics of the particles.

The LSW model assumes that ion transport between particles is diffusion-limited; however, for colloidal suspensions both diffusion and convection can contribute to ion motion. The relative influence of convective and diffusive transport is expressed by the Peclet number, Pe:[51]

$$Pe = \frac{U_0 L}{D} \quad (9)$$

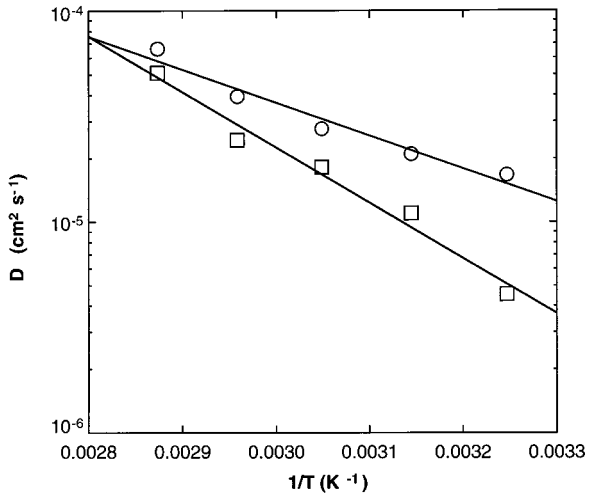

Figure 7. Arrhenius plot of the diffusion coefficient for Zn^{2+} obtained from the LSW model (□) and the Stokes−Einstein equation (○).

where U_0 is the characteristic flow velocity, L is the characteristic length along which the major change in concentration takes place, and D is the diffusion coefficient. From eq 9, it can be seen that diffusion is dominant when $Pe < 1$; conversely, when the Peclet number is large, the concentration distribution is determined by convective transport, and diffusion can be neglected. For our system, the characteristic length corresponds to the interparticle spacing which can be estimated from the particle concentration. For example, at 35 °C, taking a particle radius of 2.0 nm, the particle concentration is determined to be $\sim 10^8$ particles/cm^3, resulting in an average particle spacing of $\sim 10^{-5}$ cm. The diffusion coefficient is on the order of 2×10^{-5} cm^2/s, and from eq 9 we obtain an upper limit on the flow velocity of 2 cm/s to satisfy the condition that diffusion is dominant ($Pe < 1$). Under ambient conditions, the convective velocity is expected to be much less than this value such that molecular diffusion is expected to be the predominant mechanism of mass transport.[51]

The particle size distributions shown in Figure 2 can be compared to the distributions predicted by the LSW model.[45] The particle size distribution predicted by the LSW theory is a steady-state distribution of the form

$$f(r,t) = A\rho^2 h(\rho) \tag{10}$$

where A is a function of time and ρ is the ratio of the particle radius to the average radius, $\bar{r}$:

$$\rho = r/\bar{r} \tag{11}$$

When $\rho < {}^3/_2$, $h(\rho)$ is given by

$$h(\rho) = \left(\frac{3}{3+\rho}\right)^{7/3}\left(\frac{1.5}{1.5-\rho}\right)^{11/3}\exp\left(\frac{-\rho}{1.5-\rho}\right) \tag{12}$$

and $h(\rho) = 0$ when $\rho \geq {}^3/_2$. Following Ardell,[52] $f(\rho)$ is normalized by defining a function $g(r,t)$ such that

$$\int_0^\infty g(r,t) = 1 \tag{13}$$

Then

$$g(r,t) = \frac{\rho^2 h(\rho)}{{}^9/_4\bar{r}} \tag{14}$$

such that the theoretical time invariant function $\rho^2 h(\rho)$ is divided by ${}^9/_4\bar{r}$ for comparison with the measured histograms.

Figure 2 shows the particle size distributions for colloids aged at 35 and 65 °C for 2 h obtained from eq 14. In both cases, the mean particle size, $\bar{r}$, was obtained from analysis of the HRTEM images. Comparison of the theoretical distributions to the histograms obtained from HRTEM shows reasonable agreement although experimental data are in general broader and more symmetric than that predicted by the LSW theory. Correlation to the LSW model at the smaller particle sizes becomes difficult for particle diameters of less than about 1.5 nm where the contrast between the background of the carbon support and particles is not well defined. We note that the distributions shown in Figure 2a,b follow the LSW theory more closely than the distributions reported for other systems.[53−58]

Conclusion

The growth of ZnO particles in 2-propanol was investigated using high-resolution transmission electron microscopy, absorption spectroscopy, and X-ray diffraction. We have shown that the growth law for nanometer size ZnO particles is of the form $r = Kt^{1/3}$, consistent with Ostwald ripening kinetics. Comparison of the diffusion coefficient obtained from the constant K shows good agreement with the value predicted by the Stokes−Einstein equation. The distribution of particle sizes predicted by the LSW theory was in reasonable agreement with the distributions obtained from analysis of HRTEM images.

Acknowledgment. This work was supported by the US Army Microelectronics Research Collaboration Program. Additional support was provided by the NSF Materials Research Science and Engineering Center on Nanostructured Materials at JHU. E.M.W. acknowledges support from the JHU Materials Initiative Fellowship.

References and Notes

(1) Lianos, P.; Thomas, J. K. *Chem. Phys. Lett.* **1986**, *125* (3), 299−302.
(2) Steigerwald, M. L.; Alivisatos, A. P.; Gibson, J. M.; Harris, T. D.; Kortan, R.; Muller, A. J.; Thayer, A. M.; Duncan, T. M.; Douglass, D. C.; Brus, L. E. *J. Am. Chem. Soc.* **1988**, *110*, 3046−3050.
(3) Herron, N.; Wang, Y.; Eckert, H. *J. Am. Chem. Soc.* **1990**, *112*, 1322−1326.
(4) Rossetti, A.; Hull, R.; Gibson, J. M.; Brus, L. E. *J. Chem. Phys.* **1985**, *83* (3), 1406−1410.
(5) Alivisatos, A. P. *Science* **1996**, *271*, 933−937.
(6) Colvin, V. L.; Goldstein, A. N.; Alivisatos, A. P. *J. Am. Chem. Soc.* **1992**, *114*, 521−5230.
(7) Olshavsky, M. A.; Goldstein, A. N.; Alivisatos, A. P. *J. Am. Chem. Soc.* **1990**, *112*, 9438−9439.
(8) Brennan, J. G.; Siegrist, T.; Carroll, P. J.; Stuczynski, S. M.; Brus, L. E.; Steigerwald, M. L. *J. Am. Chem. Soc.* **1989,** *111*, 4141−4143.
(9) Kormann, C.; Bahnemann, D. W.; Hoffmann, M. R. *J. Phys. Chem.* **1988**, *92*, 5196−5201.
(10) Mittleman, D. M.; Schoenlein, R. W.; Shiang, J. J.; Colvin, V. L.; Alivisatos, A. P.; Shank, C. V. *Phys. Rev. B* **1994**, *49* (20), 14435−14447.
(11) Kortan, A. R.; Hull, R.; Opila, R. L.; Bawendi, M. G.; Steigerwald, M. L.; Carroll, P. J.; Brus, L. E. *J. Am. Chem. Soc.* **1990**, *112*, 1327−1332.
(12) Tolbert, S. H.; Herhold, A. B.; Johnson, C. S.; Alivisatos, A. P. *Phys. Rev. Lett.* **1994**, *73* (24), 3266−3269.
(13) Wang, Y.; Herron, N. *J. Phys. Chem.* **1991**, *95*, 525−532.
(14) Colvin, V. L.; Schlamp, M. C.; Alivisatos, A. P. *Nature* **1994**, *370*, 354−357.
(15) Alivisatos, A. P.; Harris, A. L.; Levinos, N. J.; Steigerwald, M. L.; Brus, L. E. *J. Chem. Phys.* **1988**, *89* (7), 4001−4011.
(16) Hoheisel, W.; Colvin, V. L.; Johnson, C. S.; Alivisatos, A. P. *J. Chem. Phys.* **1994**, *101* (10), 8455−8460.
(17) Wang, Y.; Herron, N.; Mahler, W.; Suna, A. *J. Opt. Soc. Am. B.* **1989**, *6* (4), 808−813.
(18) Fojtik, A.; Weller, H.; Koch, U.; Henglein, A. *Ber. Bunsen-Ges. Phys. Chem.* **1984**, *88*, 969−977.

(19) Herron, N.; Wang, Y.; Eddy, M. M.; Stucky, G. D.; Cox, D. E.; Moller, K.; Bein, T. *J. Am. Chem. Soc.* **1988**, *111*, 530−540.
(20) Wang, Y.; Herron, N. *J. Phys. Chem*. **1987**, *91*, 257−260.
(21) Alivisatos, A. P. *MRS Bull*. **1995**, *20* (8), 23−32.
(22) Alivisatos, A. P. *J. Phys. Chem*. **1996**, *100*, 13226−13239.
(23) Overbeek, J. Th. G. *Adv. Colloid Interface Sci*. **1982**, *15*, 2651−2677.
(24) Mahamuni, S.; Khosravi, A. A.; Kundu, M.; Kshirsagar, A.; Bedekar, A.; Avasare, D. B.; Singh, P.; Kulkarni, S. K. *J. Appl. Phys*. **1993**, *73* (10), 5237−5240.
(25) Vecht, A.; Smith, D. W.; Chadha, S S.; Gibbons, C. S.; Koh, J.; Morton, D. *J. Vac. Sci. Technol. B* **1994**, *12* (2), 781−784.
(26) Yoo, J. S.; Lee, J. D. *J. Appl. Phys.* **1997**, *81* (6), 2810−2813.
(27) Zhong, Q.; Matijevic, E. *J. Mater. Chem*. **1996**, *6*, 443−447.
(28) Sakohara, S.; Tickanen, L. D.; Anderson, M. A. *J. Phys. Chem.* **1992**, *96*, 11086−11091.
(29) Chittofrati, A.; Matijevic, E. *Colloids Surf.* **1990**, *48*, 65−78.
(30) Bahnemann, D. W.; Kormann, C.; Hoffmann, M. R. *J. Phys. Chem.* **1987**, *91*, 3789−3798.
(31) The use of brand or trade names does not imply endorsement by NIST.
(32) Brus, L. E. *J. Phys. Chem.* **1986**, *90*, 2555−2560.
(33) Brus, L. E. *J. Chem. Phys.* **1983**, *79* (11), 5566−5671.
(34) Brus, L. E. *J. Chem. Phys.* **1984**, *80* (9), 4403−4409.
(35) Brus, L. E. *Nanostruct. Mater.* **1992**, *1*, 71−75.
(36) Steigerwald, M. L.; Brus, L. E. *Acc. Chem. Res.* **1990**, *23*, 183−188.
(37) Wilson, W. L.; Szajowski, P. F.; Brus, L. E. *Science* **1993**, *262*, 1242−1244.
(38) Ramaniah, L. M.; Nair, S. V. *Physica B* **1995**, *212*, 245−250.
(39) Einvoll, G. T. *Phys. Rev. B* **1992**, *45* (7), 3410−3417.
(40) Cullity, B. D. *Elements of X-ray Diffraction*, 2nd ed.; Addison-Wesley: Reading, MA, 1978; pp 284−285.
(41) Mews, A.; Eychmuller, A.; Giersig, M.; Schooss, D.; Weller, H. *J. Phys. Chem*. **1994**, *98*, 934−941.
(42) Wang, Y.; Herron, N. *Phys. Rev. B.* **1990**, *42* (11), 7253−7255.
(43) Lippens, P. E.; Lannoo, M. *Phys. Rev. B.* **1989**, *39* (15), 10935−10942.
(44) Greenwood, G. W. *Acta Metall.* **1956**, *4*, 243−248.
(45) Lifshitz, I. M.; Slyozov, V. V. *J. Phys. Chem. Solids* **1961**, *19*, 35−50.
(46) Wagner, C. *Z. Elecktrochem.* **1961**, *65*, 581−591.
(47) Marr, D. W.; Gast, A. P. *Langmuir* **1994**, *10* (5), 1348−1350.
(48) Tremillon, B.; Inman, D. *Reactions in Solution: An Applied Analytical Approach*; John Wiley & Sons: Chichester, England, 1997; p 471.
(49) Patil, S. F.; Borhade, A. V.; Nath, M. *J. Chem. Eng. Data* **1993**, *38*, 574−576.
(50) Lovas, R.; Macri, G.; Petrucci, S. *J. Am. Chem. Soc.* **1970**, *92*, 6502−6506.
(51) Levich, V. G. *Physicochemical Hydrodynamics*; Prentice-Hall: New York, 1962; pp 49−52.
(52) Ardell, A. J. *Met. Trans*. **1970**, *1*, 525−534.
(53) Ardell, A. J. *Acta Metall.* **1972**, *20*, 61−71.
(54) Smith, A. F. *Acta Metall.* **1967**, *15*, 1867−1873.
(55) Yata, K.; Yamaguchi, T. *J. Mater. Sci.* **1992**, *27*, 101−106.
(56) Marder, M. *Phys. Rev. A* **1987**, *36* (2), 858−874.
(57) Voorhees, P. W. *Annu. Rev. Mater. Sci.* **1992**, *22*, 197−215.
(58) Ludwig, F.-P.; Schmelzer, J.; Bartels, J. *J. Mater. Sci.* **1994**, *29*, 4852−4855.